Holographic fermions with running chemical potential and dipole coupling

Li Qing Fang [1] **, Xian-Hui Ge** [1] **, Xiao-Mei Kuang**[2]

[1] *Department of Physics, Shanghai University, 200444 Shanghai, China*
[2] *Department of Physics, Shanghai Jiao Tong University, 200240 Shanghai, China*
E-mail: flqthunder@163.com, gexh@shu.edu.cn, xmeikuang@gmail.com

Abstract: We explore the properties of the holographic fermions in extremal $2+1$-charge dilatonic black hole background with a running chemical potential, as well as the dipole coupling between fermions and the gauge field in the bulk. We find that although the running chemical potential effect the location of the Fermi surface, it does not change the type of fermions. We also study the onset of the Fermi gap and the gap effected by running chemical potential and the dipole coupling. The spectral function in the limit $\omega \to 0$ and the existence of the Fermi liquid are also investigated.

Keywords: AdS/CFT Correspondence, Holographic Fermions.

Contents

1. Introduction

The gauge/gravity correspondence[1, 2, 3] is known as a powerful tool to provide key insights to disclose the mysterious phenomena observed in high temperature superconductor and heavy fermion systems, which are relative to the strongly correlated electron system. People are still lack of a general theoretical framework to deal with this so called non-Fermi liquids. Fortunately, with the use of gauge/gravity correspondence, progress has been made in our understanding of these strongly coupled system. In [4, 5, 6, 8, 7, 9], the authors has investigated the holographic Fermi surfaces. Both Fermi liquid and non-Fermi liquid are obtained by probing the behavior of the Dirac field in the RN-AdS black hole.

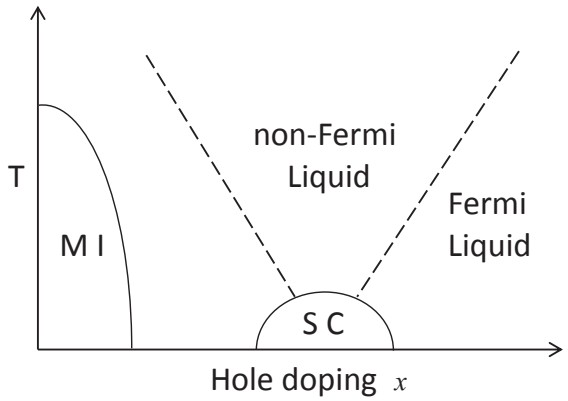

Figure 1: A schematic plot of the phase diagram of the cuprate superconductors with hole doping.

More important properties are mimicked by borrowing holography, which promotes us to understand the strongly coupled systems and the AdS/CFT correspondence deeper. One break is the observation of the transferred spectral density and the emerged Mott gap, which were archived by introducing the coupling between the fermion and gauge field through a dipole interaction in the bulk [10]. There exists a critical coupling strength at which a Mott gap opens up and continuously increasing the coupling strength makes the gap wider. More details of how the Fermi systems effect by varying the dipole coupling was also explored in [11, 12]. The bulk dipole coupling effect was also discussed in the top-down string-embedded model [13, 14]. The extended investigation on the dipole coupling in other gravity theory such as dilatonic gravity and Gauss-Bennet gravity also can be seen in[15, 16, 17]. Another but not the last break is the implementation of the holographic non-relativistic fermionic fixed points by imposing Lorentz breaking boundary conditions[18]. This makes an infinite flat band appear in the boundary field theory. The related studies on the holographic non-relativistic fermionic fixed points have been reported in [19, 20, 21, 22, 23, 24, 25, 26, 27]. In the holographic set up, the dipole coupling term seems to act as the role of "doping" in the high temperature cuprate in terms of the Hubbard model. But the physical origin of the dipole interaction term calls for further investigation.

On the other hand, the high T_c cuprate at different doping region shows its very different properties. As shown in figure 1, we can see that without doping ($x = 0$) the cuprate is the antiferromagnetic Mott insulator. By doping holes, the antiferromagnetic Mott phase is rapidly destroyed. Beyond some critical doping x_c, the non-fermi liquid phase and superconducting ground state emerges. At the over-doped region, the transition between the Fermi-liquid phase and the non-Fermi liquid phase occurs

gradually by crossover. The dopant x actually changes the chemical potential of the system. As the chemical potential running, the structure of the Fermi surfaces varies and new phases appear. So it is proper to interpret the chemical potential μ in the gravity theory as the doping x in the cuprates. It is interesting to investigate the holographic fermions with running chemical potential as "doping". In this set up, we need consider two chemical potentials, one as the background and the other as "doping".

The main motivation of the present paper is to study the effect of a running chemical potential on the probing holographic fermion system and check whether it makes a non-Fermi liquid become the Landau-Fermi type as the chemical potential runs. In [28], dilatonic black holes background with two distinct gauge fields were constructed from the top-down point of view. The authors discussed the properties of the holographic fermions with two distinct chemical potentials for various situations. Different from their work, we consider only one of the gauge fields couples with the bulk fermion and leave the other gauge field as the background. In the zero temperature limit, the two gauge fields satisfy a fixed relation and thus we can define a charge ratio. As the charge ratio varies, the chemical potential runs. Particularly, we will consider a probe Dirac fermion in the 2+1-charge dilatonic black hole[1] which involves one running chemical potential and a scalar field [28]. In order to compare the effects of the running chemical potential and the dipole coupling, the effect of the running chemical potential on the properties of the Fermi gap due to the dipole coupling between the probe fermion and either of the gauge field will also be observed. We will investigate how a running chemical potential influences on Fermi momentum and the type of Fermi liquid. We will leave the corresponding effects on the holographic non-relativistic fermionic fixed points in the future work.

The organization of this paper is as follows. In section 2, we give a brief review on the 2+1-charge dilatonic black hole solution. In section 3, we present the holographic setup of the dual fermion system in the probe setup. Then, we study the influences on the Fermi surface, the type of Fermi liquid and the Fermi gaps, due to running chemical potentials and the dipole coupling in section 4. Conclusions and discussions are presented in section 5.

2. 2+1-Charge Dilatonic Black Hole Background

The extremal 2+1-charge black holes, are the geometries obtained in [28] with two

[1] As discussed in [28], general black hole solutions in the gauged supergravity theory contain three unequal charges Q_a, Q_b and Q_c. 2+1-charge dilatonic black hole is a special situation of the black holes with two charges equal i.e., $Q_a = Q_1$ and $Q_b = Q_c = Q_2$. More details about the black hole will present in the next section.

distinct chemical potentials. For our purpose of studying running chemical potential effect, we consider the behavior of fermions in this background and later with the dipole coupling.

2.1 Review on the 2+1-charge dilatonic black hole

In this section, we will give a brief review on the 2+1-charge dilatonic black hole solution in $4+1$-dimensional spacetime, which has the form[28]

$$\begin{aligned} ds^2 &= -g_{tt}dt^2 + g_{xx}dx^2 + g_{yy}dy^2 + g_{zz}dz^2 + g_{rr}dr^2 \\ &= e^{2A(r)}[h(r)dt^2 - dx^2 - dy^2 - dz^2] - \frac{e^{2B(r)}}{h(r)}dr^2, \\ A_\mu dx^\mu &= \Phi_1(r)dt, \quad B_\mu dx^\mu = \Phi_2(r)dt, \quad \phi = \phi(r) \end{aligned} \tag{2.1}$$

with

$$\begin{aligned} A(r) &= \log(\frac{r}{L}) + \frac{1}{6}\Big(1 + \frac{Q_1^2}{r^2}\Big) + \frac{1}{3}\Big(1 + \frac{Q_2^2}{r^2}\Big), \\ B(r) &= -\log(\frac{r}{L}) - \frac{1}{3}\Big(1 + \frac{Q_1^2}{r^2}\Big) - \frac{2}{3}\Big(1 + \frac{Q_2^2}{r^2}\Big), \\ h(r) &= 1 - \frac{r^2(r_H^2+Q_1^2)(r_H^2+Q_2^2)^2}{r_H^2(r^2+Q_1^2)(r^2+Q_2^2)^2}, \\ \phi(r) &= -\sqrt{\frac{2}{3}}\log\Big(1 + \frac{Q_1^2}{r^2}\Big) + \sqrt{\frac{2}{3}}\log\Big(1 + \frac{Q_2^2}{r^2}\Big), \\ \Phi_1(r) &= \frac{Q_1(r_H^2+Q_2^2)}{2Lr_H\sqrt{r_H^2+Q_1^2}}\Big(1 - \frac{r_H^2+Q_1^2}{r^2+Q_1^2}\Big), \\ \Phi_2(r) &= \frac{Q_2\sqrt{r_H^2+Q_1^2}}{2Lr_H}\Big(1 - \frac{r_H^2+Q_2^2}{r^2+Q_2^2}\Big). \end{aligned} \tag{2.2}$$

The black brane solutions (2.1) and (2.2) are a class of solution which satisfies the effective Lagrangian with metric and matters [28]

$$e^{-1}\mathcal{L} = -R + \frac{1}{2}(\partial\phi)^2 + \frac{8}{L^2}e^{\frac{\phi}{\sqrt{6}}} + \frac{4}{L^2}e^{\frac{-2\phi}{\sqrt{6}}} - e^{\frac{-4\phi}{\sqrt{6}}}f_{\mu\nu}f^{\mu\nu} - 2e^{\frac{2\phi}{\sqrt{6}}}F_{\mu\nu}F^{\mu\nu} - 2\epsilon^{\mu\nu\rho\sigma\tau}f_{\mu\nu}F_{\rho\sigma}A_\tau \tag{2.3}$$

where $f_{\mu\nu}$ and $F_{\mu\nu}$ are the field strength of two gauge fields while ϕ is scalar field. As discussed in [28], when $Q_1 = Q_2$, the solution is a 3-charge black hole and it is a 1-charge black hole when $Q_2 = 0$. In this work, we will focus on the 2+1-charge black hole with general Q_1 and Q_2 in (2.2) where the horizon r_H satisfies $h(r_H) = 0$. Besides, the black hole background is the anti-de Sitter space in the large r limit.

The Hawking temperature of the black hole is

$$T = \frac{2r_H^4 + Q_1^2 r_H^2 - Q_1^2 Q_2^2}{2\pi L^2 r_H^2 \sqrt{r_H^2 + Q_1^2}}, \tag{2.4}$$

which will also be considered as the temperature of the system in the boundary. The chemical potentials relative to the two gauge fields read as

$$\mu_1 = \frac{Q_1(r_H^2 + Q_2^2)}{L^2 r_H \sqrt{r_H^2 + Q_1^2}}, \quad \mu_2 = \frac{\sqrt{2} Q_2 \sqrt{r_H^2 + Q_1^2}}{L^2 r_H}, \tag{2.5}$$

respectively. Moreover, the corresponding charge densities are

$$\rho_1 = \frac{Q_1 s}{2\pi r_H} \quad \text{and} \quad \rho_2 = \frac{\sqrt{2} Q_2 s}{2\pi r_H} \tag{2.6}$$

where s is the entropy density with the form

$$s = \frac{1}{4GL^3}(r_H^2 + Q_1^2)^{1/2}(r_H^2 + Q_2^2). \tag{2.7}$$

The entropy density obtained is nonzero at the zero temperature. We are interesting in the extremal black hole case, i.e., the solution with zero temperature but nonzero chemical potential. Beginning from the extremal condition, we can express Q_2 with Q_1 and r_H as

$$Q_2^2 = \frac{2r_H^4}{Q_1^2} + r_H^2. \tag{2.8}$$

To proceed, we define a dimensionless charge ratio for convenience

$$Q_R \equiv \frac{Q_1}{Q_2}. \tag{2.9}$$

By combining (2.8) and (2.9), we can re-express the two charges in terms of Q_R as

$$\begin{aligned} Q_1 &= \frac{r_H}{\sqrt{2}} \sqrt{(8Q_R^2 + Q_R^4)^{1/2} + Q_R^2}\ , \\ Q_2 &= \frac{r_H}{\sqrt{2} Q_R} \sqrt{(8Q_R^2 + Q_R^4)^{1/2} + Q_R^2}\ . \end{aligned} \tag{2.10}$$

In the following, we will set the horizon radius $r_H = 1$ and investigate the system with running chemical potentials μ_1 and μ_2 by varying the value of Q_R. The left plot of figure 2 shows us that μ_1 monotonously decreases as Q_R increases, while μ_2 is a quadratic function of Q_R and reaches its minimum at $Q_R = \sqrt{2 - \sqrt{2}} \sim 0.765$ in the right plot of figure 2. So we see that changing Q_R corresponds to varying chemical potentials. We also note that $Q_R = 1$ and $Q_R = \infty$ correspond to the 3-charge black hole and the 1-charge black hole, respectively.

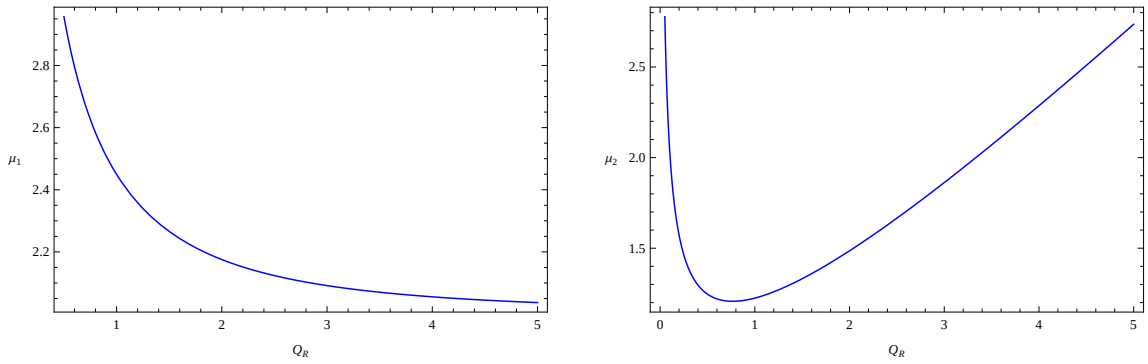

Figure 2: The plots of μ_1 (left) and μ_2 (right) versus Q_R.

2.2 Near-horizon limit

We move on to analyze the near horizon limit of the extremal 2+1-charged black hole background. Similar to the geometry discussed in [8], near the horizon region, the metric present a double pole and the geometry approaches $AdS_2 \times \mathbb{R}^3$ in the zero temperature limit. Specially, in the extremal case, the metric near the horizon has its behaviors [28]

$$\begin{aligned} g_{tt} \to -\tau_0^2 (r-r_H)^2, \quad g_{rr} \to \tfrac{L_2^2}{(r-r_H)^2}, \quad g_{xx}, g_{yy}, g_{zz} \to k_0^2, \\ \Phi_i \to \beta_i (r-r_H), \quad \phi \to \phi_0, \end{aligned} \tag{2.11}$$

where

$$\begin{aligned} \tau_0 &= \frac{2^{1/3}}{L}\Big(\frac{Q_1}{r_H}\Big)^{1/3}\sqrt{\frac{4r_H^2+Q_1^2}{r_H^2+Q_1^2}}, & L_2 &= \frac{L}{2^{2/3}}\frac{Q_1^{1/3} r_H^{2/3}}{\sqrt{4r_H^2+Q_1^2}}, \\ k_0 &= \frac{2^{1/3}}{L}\Big(\frac{r_H}{Q_1}\Big)^{2/3}\sqrt{r_H^2+Q_1^2}, & \phi_0 &= \sqrt{\frac{2}{3}}\log\Big(\frac{2r_H^2}{Q_1^2}\Big), \\ \beta_1 &= \frac{2r_H^2}{LQ_1\sqrt{r_H^2+Q_1^2}}, & \beta_2 &= \frac{Q_1\sqrt{2r_H^2+Q_1^2}}{2Lr_H\sqrt{r_H^2+Q_1^2}}. \end{aligned} \tag{2.12}$$

Then, we make the new transformations

$$r - r_H = \frac{\lambda L_2^2}{\tau_0 \zeta}, \quad t = \lambda^{-1}\tau. \tag{2.13}$$

Considering the scaling limit $\lambda \to 0$ with finite fixed ζ and τ, we find that the metric have the formulation of $AdS_2 \times \mathbb{R}^3$

$$ds^2 = \frac{L_2^2}{\zeta^2}(-d\tau^2 + d\zeta^2) + k_0^2(dx^2+dy^2+dz^2) \tag{2.14}$$

with L_2 the AdS_2 length. Meanwhile, the two gauge fields are re-scaled into the form

$$A_\mu dx^\mu = \frac{e_1}{\zeta} d\tau, \quad B_\mu dx^\mu = \frac{e_2}{\zeta} d\tau. \tag{2.15}$$

The coefficients $e_i (i = 1, 2)$ of the gauge field in the AdS_2 limit has the expression $e_i = \frac{\beta_i L_2}{\tau_0}$ with βi and τ_0 defined in (2.12). The above near horizon behavior of the background solution plays very important role when we discuss the low energy behavior of the holographic system, which will be shown in what follows.

3. Holographic Setup

In this section, we will set up the probe Fermi model in the above background. We first write down the Dirac equation in the bulk theory with the dipole coupling term. Then, we discuss the low frequency behavior of the Fermi system by using the analytical method.

3.1 Equations of motion in the bulk theory

In order to study the running chemical potential effect with dipole coupling of fermions in the dual boundary theory, we consider a probe Dirac fermion taking the mass m and charge q with the $4+1$-dimensional bulk action

$$S_{bulk} = \int d^{4+1}x\sqrt{-g} i\bar{\psi}\Big(\Gamma^a D_a - m - i\delta_{1i} p_i \not{f} - i\delta_{2i} p_i \not{F}\Big)\psi, \tag{3.1}$$

where $\Gamma^a = (e_\mu)^a \Gamma^\mu$, $\not{f} = \frac{1}{4}\Gamma^{\mu\nu}(e_\mu)^a (e_\nu)^b f_{ab}$, $\not{F} = \frac{1}{4}\Gamma^{\mu\nu}(e_\mu)^a (e_\nu)^b F_{ab}$, $\delta_{ji}(i, j = 1, 2)$ is the delta function and p_i denotes the magnetic dipole couplings strength with the two gauge fields A_μ and B_μ, respectively. The expression for the covariant derivative D_a is

$$D_a = \partial_a + \frac{1}{4}(\omega_{\mu\nu})_a \Gamma^{\mu\nu} - i\delta_{1i} q_i A_a - i\delta_{2i} q_i B_a, \tag{3.2}$$

with $\Gamma^{\mu\nu} = \frac{1}{2}[\Gamma^\mu, \Gamma^\nu]$ and the spin connection $(\omega_{\mu\nu})_a = (e_\mu)^b \nabla_a (e_\nu)_b$, where $(e_\mu)^a$ forms a set of orthogonal normal vector bases [29].

The Dirac equation derived from the above action reads

$$\Gamma^a D_a \psi - m\psi - i\delta_{1i} p_i \not{f}\psi - i\delta_{2i} p_i \not{F}\psi = 0. \tag{3.3}$$

In order to remove the spin connection in the Dirac equation and to investigate in Fourier space, following [5], we make a transformation $\psi = (-gg^{rr})^{-\frac{1}{4}} e^{-i\omega t + ik_i x^i}\phi$. Considering the rotation symmetry in the spatial directions, we can simply set $k_x = k$. The

Dirac equation (3.3) has the form

$$[\frac{\sqrt{g_{xx}}}{\sqrt{g_{rr}}}\Gamma^r\partial_r - \frac{\sqrt{g_{xx}}}{\sqrt{g_{tt}}}\Gamma^t i(\omega+\delta_{1i}q_iA_t+\delta_{2i}q_iB_t) - \sqrt{g_{xx}}m + ik\Gamma^x$$
$$-\frac{i\delta_{1i}p_i}{2}\frac{\sqrt{g_{xx}}}{\sqrt{g_{tt}g_{rr}}}\Gamma^{rt}\partial_rA_t - \frac{i\delta_{2i}p_i}{2}\frac{\sqrt{g_{xx}}}{\sqrt{g_{tt}g_{rr}}}\Gamma^{rt}\partial_rB_t]\phi = 0. \tag{3.4}$$

It is obvious that the equation above only depends on three Gamma matrices $\Gamma^r, \Gamma^t, \Gamma^x$. So it is convenient to set $\phi = \begin{pmatrix}\phi_1\\ \phi_2\end{pmatrix}$ and cosider the following basis for gamma matrices [30]:

$$\Gamma^r = \begin{pmatrix}-\sigma^3 & 0\\ 0 & -\sigma^3\end{pmatrix},\ \ \Gamma^t = \begin{pmatrix}i\sigma^1 & 0\\ 0 & i\sigma^1\end{pmatrix},\ \ \Gamma^x = \begin{pmatrix}-\sigma^2 & 0\\ 0 & \sigma^2\end{pmatrix},\ \ \cdots \tag{3.5}$$

By taking the above operations, we derive the euqation of motion (3.4)

$$\frac{\sqrt{g_{xx}}}{\sqrt{g_{rr}}}\partial_r\begin{pmatrix}\phi_1\\ \phi_2\end{pmatrix} + \sqrt{g_{xx}}m\sigma^3\otimes\begin{pmatrix}\phi_1\\ \phi_2\end{pmatrix} = \frac{\sqrt{g_{xx}}}{\sqrt{g_{tt}}}(\omega+\delta_{1i}q_iA_t+\delta_{2i}q_iB_t)i\sigma^2\otimes\begin{pmatrix}\phi_1\\ \phi_2\end{pmatrix}$$
$$\mp k\sigma^1\otimes\begin{pmatrix}\phi_1\\ \phi_2\end{pmatrix} - \frac{\delta_{1i}p_i\sqrt{g_{xx}}}{\sqrt{g_{tt}g_{rr}}}\partial_rA_t\sigma^1\otimes\begin{pmatrix}\phi_1\\ \phi_2\end{pmatrix} - \frac{\delta_{2i}p_i\sqrt{g_{xx}}}{\sqrt{g_{tt}g_{rr}}}\partial_rB_t\sigma^1\otimes\begin{pmatrix}\phi_1\\ \phi_2\end{pmatrix}. \tag{3.6}$$

Furthermore, by setting $\phi_I = \begin{pmatrix}y_I\\ z_I\end{pmatrix}$ and defining $\xi_I = \frac{y_I}{z_I}$, we decouple the equation of motion and thus reduce to

$$(\frac{\sqrt{g_{xx}}}{\sqrt{g_{rr}}}\partial_r + 2\sqrt{g_{xx}}m)\xi_I = [v_- + (-1)^Ik] + [v_+ - (-1)^Ik]\xi_I^2, \tag{3.7}$$

with $v_\pm$ expressed as

$$v_\pm = \frac{\sqrt{g_{xx}}}{\sqrt{g_{tt}}}(\omega+\delta_{1i}q_iA_t+\delta_{2i}q_iB_t) \pm \frac{\delta_{1i}p_i\sqrt{g_{xx}}}{\sqrt{g_{tt}g_{rr}}}\partial_rA_t \pm \frac{\delta_{2i}p_i\sqrt{g_{xx}}}{\sqrt{g_{tt}g_{rr}}}\partial_rB_t. \tag{3.8}$$

To solve the Dirac equation, we need impose the boundary condition. Near the AdS boundary $r\to\infty$, from the above equation, we can deduce that ϕ_I behave as

$$\phi_I \to a_Ir^{-m}\begin{pmatrix}1\\ 0\end{pmatrix} + b_Ir^m\begin{pmatrix}0\\ 1\end{pmatrix}. \tag{3.9}$$

As discussed in [6], if $a_I\begin{pmatrix}1\\ 0\end{pmatrix}$ and $b_I\begin{pmatrix}0\\ 1\end{pmatrix}$ are related by $a_I\begin{pmatrix}1\\ 0\end{pmatrix} = \mathcal{S}b_I\begin{pmatrix}0\\ 1\end{pmatrix}$, the boundary Green's functions $G(\omega,k)$ is given by $G = -i\mathcal{S}\gamma^0$. Then the Green function can be expressed as

$$G(\omega,k) = \lim_{r\to\infty} r^{2m}\begin{pmatrix}\xi_1 & 0\\ 0 & \xi_2\end{pmatrix}. \tag{3.10}$$

Up to normalization, the fermion spectral function can be written as

$$A(\omega, k) \equiv \mathrm{Tr}[\mathrm{ImG}(\omega, \mathrm{k})]. \tag{3.11}$$

On the other hand, at the horizon, we choose the in-falling boundary condition

$$\xi_I \mid_{r=r_H} = \begin{cases} i & \text{for } \omega \neq 0 \\ \frac{mL_2 - \nu_k^I}{\left(\frac{\delta_{1i} q_i \beta_i L_2}{\tau_0} + \frac{\delta_{2i} q_i \beta_i L_2}{\tau_0}\right) + \tilde{m}_I L_2} & \text{for } \omega = 0. \end{cases} \tag{3.12}$$

Here $\nu_k^I + \frac{1}{2}$ and $\tilde{m}_I$ is conformal dimension and effective mass in the low frequency theory dual to the AdS_2 background, which will be discussed in the following subsection.

3.2 Low frequency behavior

We go on to analyze the holographic system in the low frequency limit. For extremal 2+1-charge dilatonic black holes, the geometry approaches $AdS_2 \times \mathbb{R}^3$ near horizon region controlled by (2.14). In this region, we can express ϕ_I in terms of ζ and expand in powers of ω as[2]

$$\phi_I(\zeta) = \phi_I^{(0)}(\zeta) + \omega \phi_I^{(1)}(\zeta) + \omega^2 \phi_I^{(2)}(\zeta) + \cdots \tag{3.13}$$

By substituting (3.13) into (3.6), we obtain the leading order term

$$\begin{aligned} \partial_\zeta \phi_I^{(0)}(\zeta) = \frac{L_2}{\zeta} m \sigma^3 \phi_I^{(0)}(\zeta) - i\Big(1 + \frac{\delta_{1i} q_i \beta_i L_2}{\tau_0 \zeta} + \frac{\delta_{2i} q_i \beta_i L_2}{\tau_0 \zeta}\Big) \sigma^2 \phi_I^{(0)}(\zeta) \\ + \frac{L_2}{\zeta}\Big[\frac{\delta_{1i} p_i \beta_i}{\tau_0 L_2} + \frac{\delta_{2i} p_i \beta_i}{\tau_0 L_2} - (-1)^I \frac{k}{k_0}\Big] \sigma^1 \phi_I^{(0)}(\zeta). \end{aligned} \tag{3.14}$$

The above equation is identical to the equation of motion in AdS_2 background for massive spinor fields with masses $(m, \tilde{m}_I)$ where

$$\tilde{m}_I = \frac{\delta_{1i} p_i \beta_i}{\tau_0 L_2} + \frac{\delta_{2i} p_i \beta_i}{\tau_0 L_2} - (-1)^I \frac{k}{k_0} \tag{3.15}$$

are the time-reversal violating mass terms. According to the analysis in [8], $\phi_I^{(0)}(\zeta)$ is dual to the spinor operators $\mathbb{O}_I$ in the IR CFT_1 with the conformal dimensions $\delta_k^I = \nu_k^I + \frac{1}{2}$, where

$$\delta_k^I = \nu_k^I + \frac{1}{2} = \sqrt{m^2 L_2^2 + \tilde{m}_I^2 L_2^2 - \Big(\frac{\delta_{1i} q_i \beta_i L_2}{\tau_0} + \frac{\delta_{2i} q_i \beta_i L_2}{\tau_0}\Big)^2} + \frac{1}{2}. \tag{3.16}$$

[2]The low frequency limit $\omega \to 0$ is equivalent to the the scaling limit $\lambda \to 0$ in (2.13). We use ω instead of λ for unity in this section.

As in [8], the fermion retarded correlator at low frequency can be expressed with the retarded Green functions of $\mathbb{O}_I$. By matching the inner AdS_2 and outer AdS_5 solutions, we can extract the coefficients a_I and b_I in (3.9)

$$\begin{aligned} a_I &= (a_I^{(0)} + \omega a_I^{(1)} + \cdots) + (\tilde{a}_I^{(0)} + \omega \tilde{a}_I^{(1)} + \cdots)\mathcal{G}_k^I(\omega), \\ b_I &= (b_I^{(0)} + \omega b_I^{(1)} + \cdots) + (\tilde{b}_I^{(0)} + \omega \tilde{b}_I^{(1)} + \cdots)\mathcal{G}_k^I(\omega), \end{aligned} \tag{3.17}$$

with $a_I^{(n)}, \tilde{a}_I^{(n)}, b_I^{(n)}$ and $\tilde{b}_I^{(n)}$ calculated numerically and $\mathcal{G}_\alpha(k,\omega)$ the retarded Green functions of the dual operators $\mathbb{O}_I$ given by

$$\begin{aligned} \mathcal{G}_k^I(\omega) = \Big[& e^{-i\pi\nu_k^I} \frac{\Gamma(-2\nu_k^I)\Gamma(1+\nu_k^I - i\frac{\delta_{1i}q_i\beta_i L_2}{\tau_0} - i\frac{\delta_{2i}q_i\beta_i L_2}{\tau_0})}{\Gamma(2\nu_k^I)\Gamma(1-\nu_k^I - i\frac{\delta_{1i}q_i\beta_i L_2}{\tau_0} - i\frac{\delta_{2i}q_i\beta_i L_2}{\tau_0})} \\ & \times \frac{(m+i\tilde{m}_I)L_2 - i\frac{\delta_{1i}q_i\beta_i L_2}{\tau_0} - i\frac{\delta_{2i}q_i\beta_i L_2}{\tau_0} - \nu_k^I}{(m+i\tilde{m}_I)L_2 - i\frac{\delta_{1i}q_i\beta_i L_2}{\tau_0} - i\frac{\delta_{2i}q_i\beta_i L_2}{\tau_0} + \nu_k^I} \Big] \omega^{2\nu_k^I}. \end{aligned} \tag{3.18}$$

It is worthwhile to emphasize that when $2\nu_k^I$ is an integer, (3.17) is invalid and an additional terms should be considered[8].

4. Properties of the Fermion System with Running Chemical Potential and the Dipole Coupling

We are going to explore the properties of the holographic system by numerically integrating the flow equation (3.7). We will calculate the fermion spectral function $A(\omega, k)$ defined in (3.11) and the density of states $A(\omega)$ by doing the integration of $A(\omega, k)$ over k. Note that from figure 2, it is obvious that μ_1 and μ_2 depend on Q_R with different rules, so we will discuss both the fermi surface and the gap for the two cases that A_t and B_t couple to probe fermions separately. For the convenience of our numerical calculation, we will set $m = 0$, $L = 1$, $r_H = 1$ and $q_i = 2$.

4.1 Fermi surface without dipole interaction

Firstly, we consider the the minimal dipole coupling with $p_i = 0 (i = 1, 2)$ and discuss the Fermi momentum k_F where the retarded Green functions has a sharp quasi-particle-like peak. Before going on, we would like to point out that the Green function has a symmetry $G_{22}(\omega, k) = G_{11}(\omega, -k)$ which can be easily seen from the (3.7) and the boundary condition (3.12). Thus, we mainly focus on studying $G_{22}(\omega, k)$.

Q_R	0.5	1	1.5	2	2.5	3
k_F	–	1.6710	1.1983	0.8674	0.6169	0.4679
α	–	3.37034	3.81993	5.38319	8.4646	12.2274
(ν_k)	–	(0.148347)	(0.130892)	(0.0928817)	(0.0590695)	(0.0408916)

Table 1: k_F and α with different chemical potential at $p_1 = 0$ for $i = 1$.

4.1.1 Case I: Only A_t couples with the probe fermions

Let us consider the case that only the gauge field A_t interacts with the probe Dirac fermion. That is to say, we will choose $i = 1$ in (3.1) and (3.2). For the minimal dipole coupling, we examine the fermi surface carefully and discover that there exists a quasi-particle-like peak for some samples of Q_R. Specially, in the left panel of Figure 3, we shows the behaviors of $\mathrm{ImG}_{22}(\mathrm{k})$ for some samples of Q_R with $\omega = -10^{-11}$. We see that the Fermi momentum k_F becomes smaller for bigger Q_R. The more precise values of k_F are summarized in Table 1. When $Q_R < 0.5$, ν_k is imaginary, so the Fermi surface does not exist. This tells us, in the log-oscillatory regime $Q_R < 0.5$ and $p_1 = 0$, there is no real Fermi surfaces.

In order to estimate the character of dual liquid, we need to check the behavior of ImG_{22} near the Fermi momentum $k_\perp = k - k_F$, named dispersion relation of the Green function ImG_{22}. The dispersion relation can be expressed as

$$\omega_*(k_\perp) \sim k_\perp^\alpha, \tag{4.1}$$

where $\omega_*(k_\perp)$ is the distance to the location of Fermi surface and the scaling exponent α can be determined by

$$\alpha = \begin{cases} 1 & \text{when } \nu^I_{k_F} > \frac{1}{2} \\ \frac{1}{2\nu^I_{k_F}} & \text{when } \nu^I_{k_F} < \frac{1}{2} \end{cases} \tag{4.2}$$

with $\nu^I_{k_F}$ easily obtained from (3.16) at $k = k_F$. As we know when $\nu^I_{k_F} > \frac{1}{2}$ ($\alpha = 1$), the dual liquid corresponds to Fermi liquid. When $\nu^I_{k_F} < \frac{1}{2}$, the dual liquid corresponds to non-Fermi liquid. After determining the Fermi momentum, we analytically calculate the scaling exponent α via (3.16) and (4.2). The results in Table 1 reveal that the dual holographic system is always non-Fermi liquid as the chemical potential changes. It seems that the change of chemical potential has no influence on the fundamental type of the dual liquid.

4.1.2 Case II: Only B_t couples with the probe fermions

Then we turn to study the other case that only the gauge field B_t couples with bulk fermions while A_t is a part of background. The chemical potential μ_2 relative to B_t is not monotonous in the positive region of Q_R. The decreasing and increasing interval

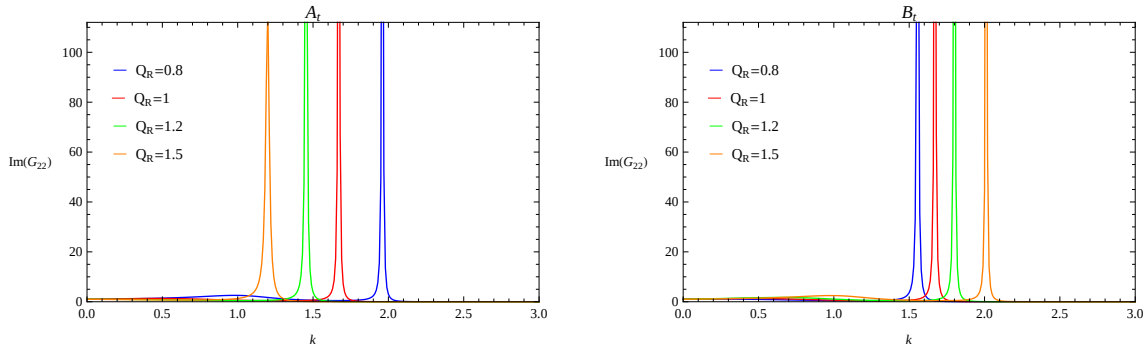

Figure 3: The plot of ImG$_{22}$(k) for $Q_R = 0.8$(blue), $Q_R = 1$(red), $Q_R = 1.2$(green) and $Q_R = 1.5$(orange).

Q_R	0.1	0.2	0.5	0.765	1	1.5	2
k_F	1.6870	1.4665	1.4268	1.5377	1.6710	2.0111	2.3975
α	3.7955	3.56655	3.33173	3.31293	3.37049	3.6601	4.15051
(ν_k)	(0.131735)	(0.140191)	(0.150072)	(0.150924)	(0.148347)	(0.136608)	(0.120467)

Table 2: k_F and α with different chemical potential at $p_2 = 0$ for case $i = 2$.

of μ_2 are the regions of $0 < Q_R < 0.765$ and $Q_R > 0.765$, respectively. We find that Fermi momentum increases as Q_R increases in the region of $Q_R > 0.765$ but the rule does not hold in the complementary region. The location of the Fermi surface is shown in the right panel of Figure 3 while the values of k_F and the critical exponents are summarized in Table 2. From this numerical result, it seems that different from that in the previous case, and in this case the Fermi momentum has no consistent rule as the chemical potential changes. Nonetheless, the similar result to that in the case of nonzero A_t is that the type of dual system is also always non-Fermi liquid.

From the above discussion with the minimal dipole coupling, let us give a short summary: Firstly, the chemical potential has influence on the Fermi momentum when either of the gauge field A_t or B_t interacts with the probe fermion. Secondly, the chemical potential effects the scaling exponent of dispersion relation, but it can not change the type of dual non-Fermi liquid. The result is reasonable because the electric field is actually hidden behind the horizon for the charged black hole. So the system violates the Luttinger's theorem [31].

4.2 Various properties with nonvanishing dipole coupling

Now we turn on the dipole coupling term. We will investigate the influence of the dipole coupling constant p_i and chemical potential on the dual system. In order to achieve this goal, we will explore the density of states by integrating $A(\omega, k)$ over k. We will

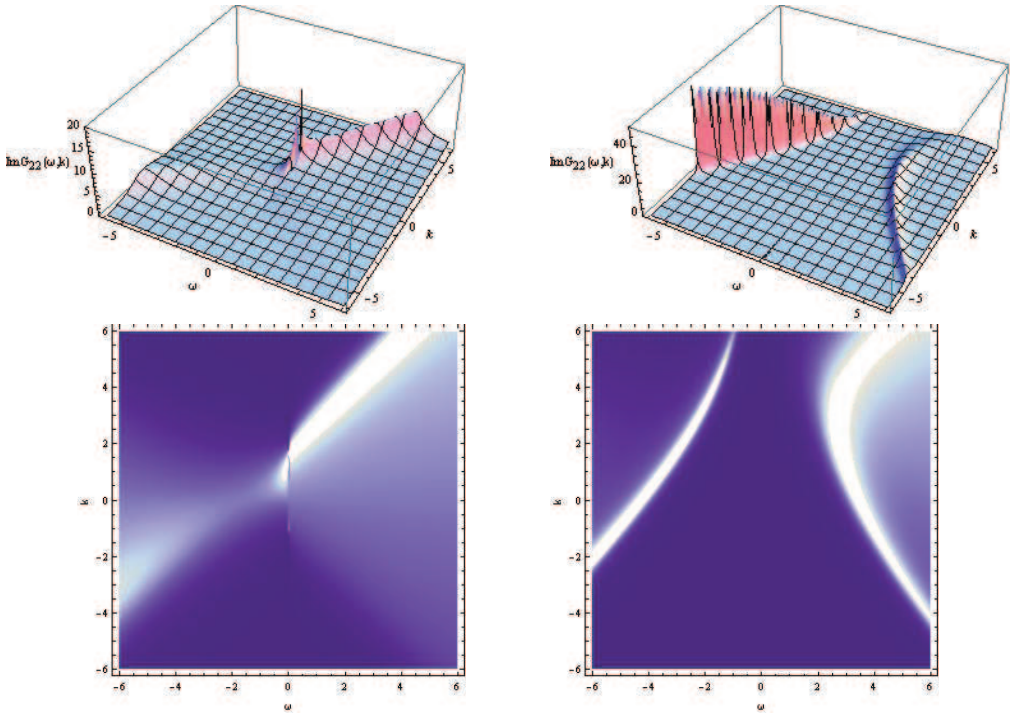

Figure 4: The 3D plot of $\mathrm{ImG}_{22}(\omega, \mathrm{k})$ and its density plot for $p_1 = 0$ (left plane) and $p_1 = 5$ (right plane). We set $q_1 = 2$ and $Q_R = 1$.

use different values of Q_R for discussion in this section since changing Q_R is equivalent to a running chemical potential.

4.2.1 A_t interacts with the probe fermion

At first, we focus on the case that only A_t couples with the probe fermions. In other word, we will set $i = 1$ in (3.7). In figure 4, the plots show $\mathrm{ImG}_{22}(\omega, \mathrm{k})$ for $p_1 = 0$(left panel) and $p_1 = 5$(right panel) with $Q_R = 1$. The left plots for $p_1 = 0$ show the same result as we analyzed in previous section that the quasi-particle-like peak representing a Fermi surface locates at $k \simeq 1.67$ as $\omega \to 0$. The low energy excitations near k_F are non-Fermi liquid type. However, from the right plots for $p_1 = 5$, we find the peak around $\omega \to 0$ disappear and a gap generated.

For small p_1, the major feature of the system is that the spectral function has a quasi-particle-like peak which locates at $k = k_F$. As p_1 increases, the peak declines. Once p_1 reaches a critical value p_{1cri}, a gap will emerge. The width of gap will become larger as p_1 increases further. Also the peaks initiate to transfer from the upper band with $\omega > 0$ to the lower band with $\omega < 0$. From the state density versus the frequency

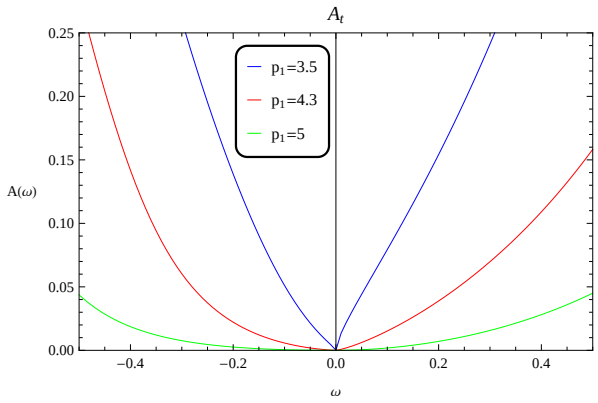

Figure 5: The plot of $A(\omega)$ for $p_1 = 3.5$(blue line), $p_1 = 4.3$(red line) and $p_1 = 5$(green line). The onset of the gap is near $p_1 = 4.3$ with $Q_R = 1$.

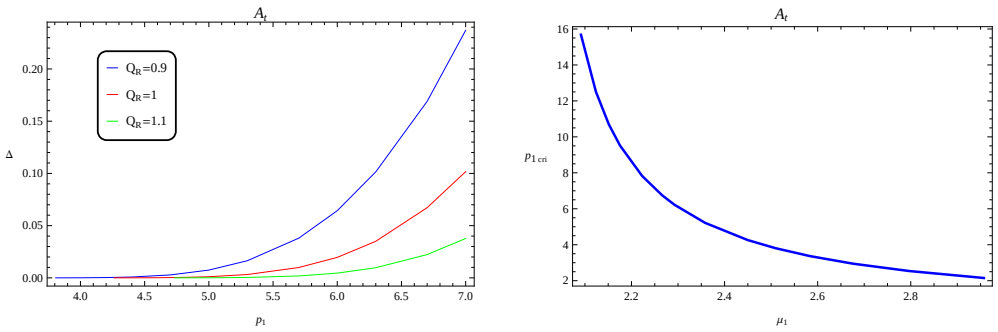

Figure 6: Left: The plot of gap width versus p_1 for different Q_R. Right: P_{1cri} as a function of μ_1.

in figure 5, we can see the onset of gap is near $p_{1cri} = 4.3$ with $Q_R = 1$[3]. The transfer of the spectral density is also implicit in the figure. Furthermore, the width of the gap enlarging with p_1 can also be seen in the left plot of figure 6. In the right plot of figure 6, we show the effect of the chemical potential on the critical dipole coupling. We see that smaller chemical potential makes the generation of gap at larger dipole coupling. In other words, the relative chemical potential change the effect of dipole coupling. Other factor that change the dipole coupling effect also discussed in [15, 16, 17].

In order to see more influence on the holographic fermion system by the running chemical potential, we report our numerical result in the limit when $\omega = 0$ with different Q_R in figure 7. From the figure, it is obvious that the symmetry of $\mathrm{ImG}_{11}(0, -\mathrm{k}) = \mathrm{ImG}_{22}(0, \mathrm{k})$ is kept for both $p_1 = 0$ and $p_1 = 0.1$. Besides, there is a range of k

[3]We integrate $A(\omega)$ over k in sufficiently wide range. When the value of $A(\omega)$ reaches 4.5×10^{-8}, we deem the spectral function $A(\omega) \sim 0$ accompanying the gap generates at p_{1cri}.

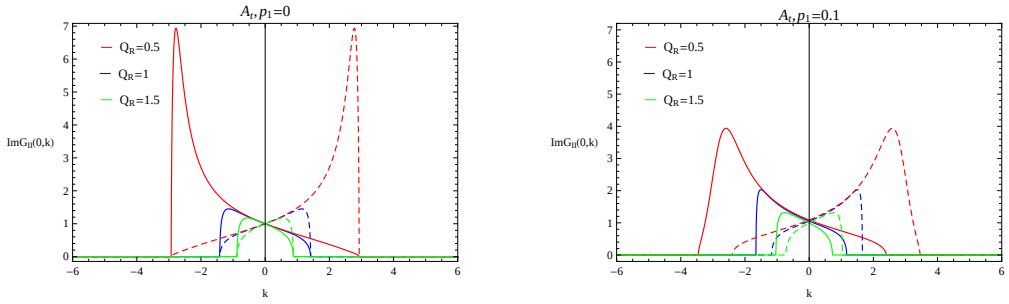

Figure 7: $\mathrm{ImG}_{11}(0,\mathrm{k})$(dashed) and $\mathrm{ImG}_{22}(0,\mathrm{k})$(solid) for $p_1 = 0$ and $p_1 = 0.1$ with various Q_R.

in which both $\mathrm{ImG}_{11}(0,\mathrm{k})$ and $\mathrm{ImG}_{22}(0,\mathrm{k})$ are nonzero. This range of k at fixed p_1 becomes wider as Q_R becomes smaller. As pointed out in[5], $\mathrm{ImG}_{\mathrm{II}}(\omega,\mathrm{k})$ becomes log-oscillatory when ω approaches zero in the momentum regime for nonzero $\mathrm{ImG}_{\mathrm{II}}(0,\mathrm{k})$. The left plot of figure 7 shows that the log-oscillatory regimes coincide at $p_1 = 0$ for all chosen Q_R. While this coincidence will shrink for bigger p_1 as shown in the right plot of figure 7.

Fortunately, we can analytical understand the above properties of the log-oscillatory regimes. By studying the conformal dimension ν_k^I of the dual CFT operator, we find there is a range of momenta $k \in \mathcal{X}_I$ in which ν_k^I is imaginary. The momentum regime with imaginary ν_k^I corresponds to the log-oscillatory regime[8] and Fermi surface do not occur in this regime. In our model, we have the range of log-oscillatory regime from (3.16)

$$k \in \mathcal{X}_I = \Big[\frac{(-1)^I(\delta_{1i}\beta_i k_0 p_i + \delta_{2i}\beta_i k_0 p_i) - (\delta_{1i} q_i k_0 \beta_i L_2 + \delta_{2i} q_i k_0 \beta_i L_2)}{L_2 \tau_0}, \\ \frac{(-1)^I(\delta_{1i}\beta_i k_0 p_i + \delta_{2i}\beta_i k_0 p_i) + (\delta_{1i} q_i k_0 \beta_i L_2 + \delta_{2i} q_i k_0 \beta_i L_2)}{L_2 \tau_0}\Big]. \tag{4.3}$$

For $k \in \mathcal{X}_I$, our boundary condition (3.12) with $\omega = 0$ is imaginary while the flow equation is real, so the numerical result in figure 7 that $\mathrm{ImG}_{\mathrm{II}}(0,\mathrm{k})$ is nonzero in this momentum regime is obvious. Also, it is easy to see from (4.3) that $\mathcal{X}_1 = \mathcal{X}_2$ for $p_1 = 0$. While for nonzero p_1, $\mathcal{X}_1$ and $\mathcal{X}_2$ will be different, both of $\mathrm{ImG}_{\mathrm{II}}(\omega,\mathrm{k})$ are oscillatory only when the values of k belongs to the overlap of $\mathcal{X}_1$ and $\mathcal{X}_2$. This support the coincidence and separation of the log-oscillatory regime in figure 7. The separations of the regimes $\mathcal{X}_1$ and $\mathcal{X}_2$ for chosen Q_R are plotted in figure 8, we can see that the smaller chemical potential corresponds to wider log-oscillatory regimes. The analytical results support and explain the numerical result perfectly.

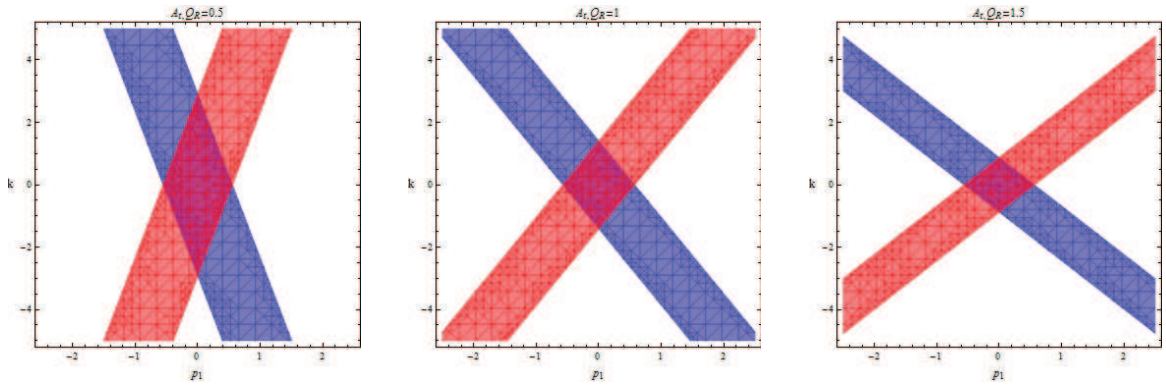

Figure 8: The plots of oscillating region for different Q_R.

	$p_1 = -1$	$p_1 = -0.1$	$p_1 = 0$	$p_1 = 0.1$	$p_1 = 0.2$	$p_1 = 0.5$	$p = 5$
$Q_R = 0.9$	$k_F = 1.02993$ $\alpha = 1$ FL	$k_F = 1.68641$ $\alpha = 2.60958$ NFL	$k_F = 1.80341$ $\alpha = 3.51576$ NFL	$k_F = 1.93739$ $\alpha = 6.11777$ NFL	NFS	NFS	MI
$Q_R = 1$	$k_F = 0.91896$ $\alpha = 1$ FL	$k_F = 1.56377$ $\alpha = 2.66054$ NFL	$k_F = 1.67102$ $\alpha = 3.37034$ NFL	$k_F = 1.79031$ $\alpha = 4.81534$ NFL	$k_F = 1.92277$ $\alpha = 13.0162$ NFL	NFS	MI
$Q_R = 1.1$	$k_F = 0.81924$ $\alpha = 1.09611$ NFL	$k_F = 1.45591$ $\alpha = 2.74919$ NFL	$k_F = 1.55604$ $\alpha = 3.34608$ NFL	$k_F = 1.66506$ $\alpha = 4.37043$ NFL	$k_F = 1.78357$ $\alpha = 6.90966$ NFL	NFS	MI

Table 3: The Fermi momentum k_F and the exponent α of dispersion relation with different p and various Q_R for A_t. NFS means the system doesn't present Fermi surface. FL, NFL and MI denote Fermi liquid, non-Fermi liquid and Mott insulator, respectively.

We summarize the phase structure of the holographic fermions coupled with A_t field in table 3. When we change the value of p_1 from small positive to negative, the excitation near the Fermi surface can change from non-Fermi Liquid to Fermi Liquid. Note that "NFS" means ν_k is imaginary where Fermi surface do not occur. We also find that when $p_1 = -1$, decreasing chemical potential can make the dual Fermi liquid system change to non-Fermi liquid.

4.2.2 B_t interacts with the probe fermion

We also do some parallel work in the case that only B_t couples with bulk fermions (i.e. i=2). The results are shown in figure 9-11. To no one's surprise, there also exists Fermi surface. In figure 9, p_{cri} of the onset of the gap will change with the change of the chemical potential. But the features are quite different from that in the case of μ_1, because μ_2 is a quadratic function of the chargeless ratio Q_R. So μ_2 is also a quadratic function of p_{cri}.

The properties of the log-oscillatory regimes is also worth studying. Figure 10 is

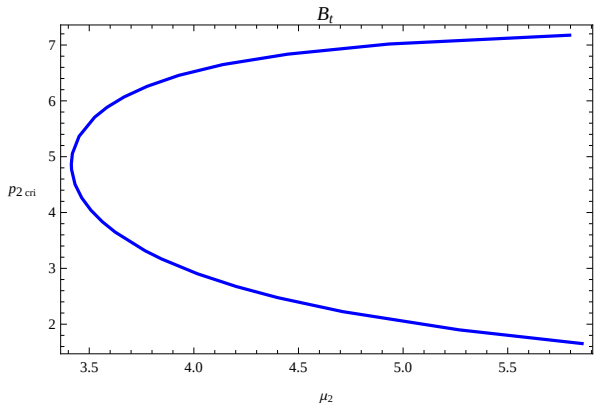

Figure 9: P_{2cri} as a function of μ_2 for the B_t case.

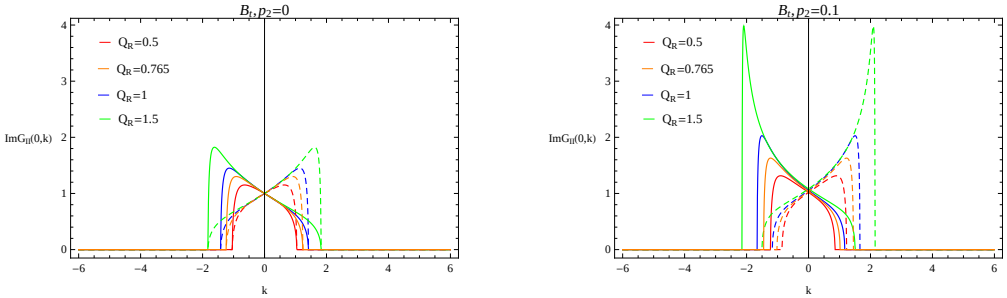

Figure 10: $\mathrm{ImG}_{11}(0,\mathrm{k})$(dashed) and $\mathrm{ImG}_{22}(0,\mathrm{k})$(solid) for $p_2 = 0$ and $p_2 = 0.1$ with various Q_R for B_t case.

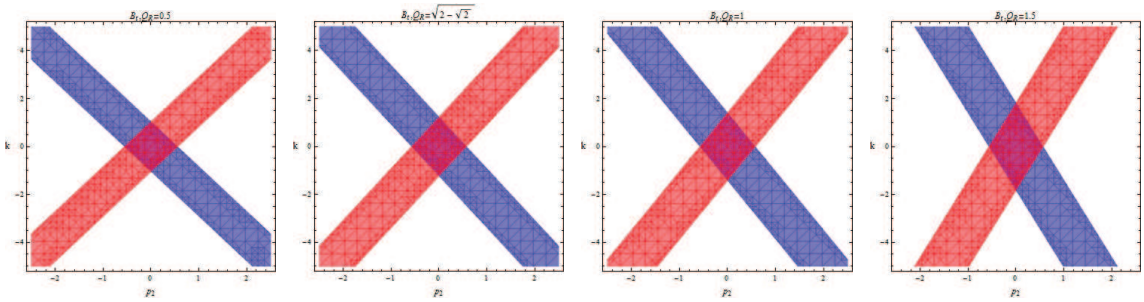

Figure 11: The plots of oscillating region with different Q_R for B_t case.

the numerical result given by using the $\omega = 0$ boundary condition (3.12). It shows the log-oscillatory regimes is narrower when Q_R increase. Figure 11 is the corresponding analytical result, which also agrees well with the numerical results on the width of the log-oscillatory regimes. The separation of the regimes $\mathcal{X}_1$ and $\mathcal{X}_2$ is smaller as Q_R enlarges.

	$p_2 = -1$	$p_2 = -0.1$	$p_2 = 0$	$p_2 = 0.1$	$p_2 = 0.2$	$p_2 = 0.5$	$p = 5$
$Q_R = 0.9$	$k_F = 0.86751$ $\alpha = 1.04006$ NFL	$k_F = 1.50811$ $\alpha = 2.69864$ NFL	$k_F = 1.61142$ $\alpha = 3.33878$ NFL	$k_F = 1.72495$ $\alpha = 4.51229$ NFL	$k_F = 1.84952$ $\alpha = 8.16924$ NFL	NFS	MI
$Q_R = 1$	$k_F = 0.91896$ $\alpha = 1$ FL	$k_F = 1.56377$ $\alpha = 2.66054$ NFL	$k_F = 1.67102$ $\alpha = 3.37034$ NFL	$k_F = 1.79031$ $\alpha = 4.81534$ NFL	$k_F = 1.92277$ $\alpha = 13.0162$ NFL	NFS	MI
$Q_R = 1.1$	$k_F = 0.97232$ $\alpha = 1$ FL	$k_F = 1.62246$ $\alpha = 2.62679$ NFL	$k_F = 1.73398$ $\alpha = 3.41129$ NFL	$k_F = 1.85959$ $\alpha = 5.21841$ NFL	NFS	NFS	MI

Table 4: The Fermi momentum k_F and the exponent α of dispersion relation with different p and various Q_R for B_t.

The phase structure of holographic fermions coupled with only B_t field is shown in table 4. We also find the similar phenomena with the A_t case that bigger charge ratio Q_R can help the type of the dual system change from Fermi liquid to non-Fermi liquid.

5. Conclusions and Discussions

Inspired by the phase diagram of the high T_c cuprates, we have shown the influence of the running chemical potential on the dual fermion system in the 2+1-charge dilatonic geometry. In the minimal dipole coupling, the running chemical potential directly proportional to the Fermi momentum both for two gauge fields A_t and B_t. No matter what changes on the running chemical potential, the properties of the dual system are the non-Fermi liquid type. This is consistent with the argument given in [31] that charges hidden behind the horizon lead to the violation of the Luttinger's theorem and thus result in non-Fermi liquid. We also discussed the non-vanishing dipole coupling effect. As to the Dirac operator coupled with only the A_t field case, the bigger chemical potential makes the generation of the gap easier. When only B_t field interacts with the bulk fermions, we found that μ_2 is a quadratic function of the critical dipole coupling constant P_{2cri}. We noted that μ_1 corresponds to one black hole charge case and μ_2 corresponds to two equal charges, which probably play a role in the diagrams of the μ_i-$P_{i\ cri}$ relation. But the specific reason need us to do further research. We also plot the phase structure for the holographic fermions for both the A_t and B_t cases with dipole coupling. We found that when we turn on dipole coupling, the running chemical potential can influence the type of the dual liquid. In summary, the presence of the running chemical potential and the dipole coupling enrich the physical picture of the holographic fermions.

Acknowledgements

We would like to thank Bin Wang for encouragement. The work was partly supported by NSFC (No. 11075036 and No. 11005072). XHG was also partly supported by Shanghai Rising-Star Program (No.10QA1402300).

References

[1] J. M. Maldacena, "The Large N Limit of Superconformal Field Theories and Supergravity ", Adv. Theor. Math. Phys. 2, 231 (1998), [arXiv:hep-th/9711200].

[2] S. S. Gubser, I. R. Klebanov and A. M. Polyakov, "Gauge Theory Correlators from Non-Critical String Theory", Phys. Lett. B 428, 105 (1998), [arXiv:hep-th/9802109].

[3] E. Witten, "Anti De Sitter Space And Holography ", Adv. Theor. Math. Phys. 2, 253 (1998), [arXiv:hep-th/9802150].

[4] S. S. Lee, "A Non-Fermi Liquid from a Charged Black Hole; A Critical Fermi Ball", Phys. Rev. D 79 (2009) 086006, [arXiv:0809.3402].

[5] H. Liu, J. McGreevy and D. Vegh, "Non-Fermi liquids from holography", Phys. Rev. D 83 (2011) 065029, [arXiv:0903.2477].

[6] N. Iqbal and H. Liu, "Real-time response in AdS/CFT with application to spinors", Fortsch. Phys. 57, 367 (2009), [arXiv:0903.2596].

[7] M. Cubrovic, J. Zaanen and K. Schalm, "String Theory, Quantum Phase Transitions and the Emergent Fermi-Liquid", Science 325 (2009) 439, [arXiv:0904.1993].

[8] T. Faulkner, H. Liu, J. McGreevy and D. Vegh, "Emergent quantum criticality, Fermi surfaces, and AdS2," Phys. Rev. D 83 (2011) 125002, [arXiv:0907.2694].

[9] T. Faulkner, N. Iqbal, H. Liu, J. McGreevy, and D. Vegh, "Strange metal transport realized by gauge/gravity duality", Science 329 (2010) 1043-1047, [arXiv:1003.1728].

[10] M. Edalati, R. G. Leigh, P. W. Phillips, "Dynamically Generated Gap from Holography: Mottness from a Black Hole", Phys. Rev. Lett. 106, 091602 (2011), [arXiv:1010.3238].

[11] M. Edalati, R. G. Leigh, K. W. Lo, P. W. Phillips, "Dynamical Gap and Cuprate-like Physics from Holography", Phys. Rev. D 83, 046012 (2011), [arXiv:1012.3751].

[12] D. Guarrera, J. McGreevy, "Holographic Fermi surfaces and bulk dipole couplings", [arXiv:1102.3908].

[13] J. P. Gauntlett, J. Sonner, D. Waldram, "Universal fermionic spectral functions from string theory", Phys. Rev. Lett. 107, 241601 (2011), [arXiv:1106.4694].

[14] J. P. Gauntlett, J. Sonner, D. Waldram, "Spectral function of the supersymmetry current", JHEP 11 (2011) 153, [arXiv:1108.1205].

[15] J. P. Wu, H. B. Zeng, "Dynamic gap from holographic fermions in charged dilaton black branes", JHEP 1204 (2012) 068, [arXiv:1201.2485].

[16] W. Y. Wen, S. Y. Wu, "Dipole Coupling Effect of Holographic Fermion in Charged Dilatonic Gravity", Phys.Lett. B712 (2012) 266-271, [arXiv:1202.6539].

[17] X. M. Kuang, B. Wang, J. P. Wu, "Dipole Coupling Effect of Holographic Fermion in the Background of Charged Gauss-Bonnet AdS Black Hole", JHEP 07 (2012) 125, [arXiv:1205.6674].

[18] J. N. Laia, D. Tong, "A Holographic Flat Band", JHEP 11 (2011) 125, [arXiv:1108.1381].

[19] J. N. Laia, D. Tong, "Flowing Between Fermionic Fixed Points", JHEP 11 (2011) 131, [arXiv:1108.2216].

[20] W. J. Li, H. Zhang, "Holographic non-relativistic fermionic fixed point and bulk dipole coupling", JHEP 11 (2011) 018, [arXiv:1110.4559].

[21] W. J. Li, R. Meyer, H. Zhang, "Holographic non-relativistic fermionic fixed point by the charged dilatonic black hole", JHEP 01 (2012) 153, [arXiv:1111.3783].

[22] U. Gursoy, E. Plauschinn, H. Stoof, S. Vandoren, "Holography and ARPES sum-rules", JHEP 05 (2012) 018, [arXiv:1112.5074]

[23] M. Alishahiha, M. R. M. Mozaffar, A. Mollabashi, "Fermions on Lifshitz Background", Phys. Rev. D 86, 026002 (2012), [arXiv:1201.1764].

[24] L. Q. Fang, X. H. Ge and X. M. Kuang, "Holographic fermions in charged Lifshitz theory", Phys. Rev. D 86, 105037 (2012), [arXiv:1201.3832].

[25] W. J. Li, J. P. Wu, "Holographic fermions in charged dilaton black branes", Nuclear Physics B, 867 (2013), 810-826, [arXiv:1203.0674].

[26] U. Gursoy, V. Jacobs, E. Plauschinn, H. Stoof, S. Vandoren, "Holographic models for undoped Weyl semimetals", [arXiv:1209.2593]

[27] X. M. Kuang, B. Wang, J. P. Wu, "Dynamical gap from holography in the charged dilaton black hole", [arXiv:1210.5735].

[28] O. DeWolfe, S. S. Gubser, C. Rosen, "Fermi surfaces in N=4 Super-Yang-Mills theory", Phys. Rev. D.86.106002, [arXiv:1207.3352].

[29] R. M. Wald, "General Relativity", University of Chicago Press, Chicago, U.S.A. (1984)

[30] T. Faulkner, G. T. Horowitz, J. McGreevy, M. M. Roberts, D. Vegh, JHEP 03 (2010) 121, [arXiv:0911.3402].

[31] N. Iqbal, H. Liu, "Luttinger's theorem, superfluid vortices, and holography," Class. Quant. Grav. 29, 194004 (2012), [arXiv:1112.3671].